J. Fluid Mech. (1989), *vol.* 199, *pp.* 541–561
Printed in Great Britain

Measurements of heat transfer in separated high-enthalpy dissociated laminar hypersonic flow behind a step

By S. L. GAI, N. T. REYNOLDS, C. ROSS AND J. P. BAIRD
University College, UNSW, Australian Defence Force Academy, Canberra, Australia

(Received 19 May 1987 and in revised form 17 July 1988)

Measurements of heat transfer in the separated region behind a rearward-facing step in a hypersonic high-enthalpy stream, are described. The range of enthalpies considered was much greater than those reported previously in the literature. High-response surface thermocouples were used to measure the heat-transfer rates. Flow visualization by way of interferograms, with a Mach–Zehnder interferometer, were obtained and improved visualization was further facilitated by digitizing the interferograms and using Fourier analysis to determine fringe positions. This then provided a phase map of the flow region in which the phase was colour coded to emphasize flow characteristics.

1. Introduction

In order to gain an understanding of the separated flow behind re-entry-type vehicles flying at hypervelocities, detailed knowledge of heat transfer and pressure field are necessary but such data are sparse (Nestler 1985). As the simplest example of non-equilibrium hypersonic separated flow, the flow past a rearward-facing step has been studied in this paper.

The flow past a rearward-facing step in hypersonic flow is characterized by a strong expansion round the corner of the step. This significantly influences the downstream separated region, particularly causing a large growth of the shear layer, which affects pressure and heat-transfer rates (Shang & Korkegi 1968; Wada & Inoue 1973).

In the present study of a two-dimensional rearward-facing step in hypersonic high-enthalpy flow, emphasis is placed on heat-transfer measurements using micro-second-response surface thermocouples and flow visualization using Mach–Zehnder interferometry. Improved flow visualization was further facilitated by digitizing the interferograms and using Fourier analysis to determine fringe positions. This provides a phase map of the flow region in which the phase is colour coded to emphasize the flow characteristics.

2. Facility, experimental conditions, model and instrumentation

2.1. *Facility and experimental conditions*

The tests were conducted at the Australian National University free-piston-driven shock tunnel T3 with air as test gas and helium as driver gas. The flow was generated through a conical nozzle of 305 mm exit diameter and 12.5 mm throat. This provided a test gas of frozen composition in the Mach-number range of 7.7 to 10 depending on

the stagnation enthalpy and the stagnation pressure. The tunnel was operated at three different conditions. These conditions are designated as run types B, D and G (see East, Stalker & Baird, 1980) and were typical of high-, medium and low-enthalpy flow respectively.

While the free-piston shock tunnels at the Australian National University are unique in their ability to generate velocities in air equivalent to re-entry speeds and sufficient to cause dissociation of oxygen and nitrogen molecules, the testing environment differs from the flight environment in two important aspects. First, the free stream is a frozen dissociated flow for the higher enthalpy tests. For example, in the present context, at condition B, most of the oxygen and a small fraction of nitrogen was dissociated into oxygen and nitrogen atoms. At condition D, nearly $\frac{2}{3}$ of the oxygen (but no nitrogen) was dissociated, while for the low-enthalpy condition G, there was no dissociation.

Secondly, short run times of a few hundred microseconds or so (typically 800 μs to 1000 μs) are not sufficient to allow equilibration of the surface temperature of the models. As a result the wall is much colder than in real flight vehicles. Nevertheless, reaction distance to model length ratios similar to flight conditions at typical re-entry altitudes can be achieved (Stalker 1985).

The free-stream conditions at the exit plane of the nozzle were obtained, first by calculating the nozzle reservoir conditions from the measured shock speed and the reservoir pressure, taking the gas to be in thermodynamic equilibrium. From these reservoir conditions, the non-equilibrium flow through the conical nozzle was then determined using a computer programme based on the method of Lordi, Mates & Moselle (1966) for one-dimensional non-equilibrium gas expansions. Extensive measurements by R. J. Stalker (1982, personal communication) made in the shock tunnel T3 have confirmed that the calculated free-stream conditions and stagnation enthalpies are realized in the test section. Detailed mass-spectrometric studies by Crane & Stalker (1977) have shown that for stagnation enthalpies up to 25 MJ/kg helium driver gas contamination is not a problem but for higher enthalpies a penalty has to be paid in terms of reduced test times.

The flow conditions that the model was subjected to are summarized in table 1. The model wall temperature (T_w) was taken to be 300 K ambient. The free-stream Mach number (M_∞) is based on the free-stream speed (U_∞) and the frozen speed of sound (a_f), with $a_f = (\gamma_f R_\infty T_\infty)^{\frac{1}{2}}$, where γ_f is the frozen specific heat ratio and R_∞ is a gas constant based on calculated flow composition at the exit plane of the nozzle.

The Reynolds numbers based on free-stream conditions per m and viscosity μ_∞ calculated following East *et al.* (1980) varied from 29.5×10^4 to 46.6×10^5. The values of viscosity are based on an equilibrium mixture and calculated using the Lennard–Jones intermolecular potential model. Based on the upstream plate length (figure 1) the Reynolds number varied from about 1×10^4 to 23×10^4.

2.2. *Model and instrumentation*

A steel model with a sharp leading edge and a back step located about 50 mm downstream was used for the experiments. Downstream of the step the plate was extended by 150 mm.

The tests were conducted using two step heights of 6 mm and 3 mm. In the latter case, however, in view of the way the model was constructed, the upstream plate length was reduced from 50 mm to 33 mm.

The aspect ratio of the model (that is, the ratio of width to chord) for the two

Run type	Stagn. press p_0 (atm)	Stagn. enthalpy h_0 (MJ/kg)	Equilib. stagn. temp. T_0 (K)	Wall to stagn. temp. ratio T_w/T_0	Free-stream conditions: Velocity U_∞ (km/s)	Density $\rho_\infty \times 10^3$ (kg/m^3)	Temp. T_∞ (K)	M_∞	γ_f	Re_∞/m
B	260	19.8	8645	0.0347	5.6	2.37	1140	7.8	1.45	29.5×10^4
D	210	13.6	7178	0.0418	4.7	2.65	870	7.7	1.43	33×10^4
G	170	2.6	2268	0.132	2.1	12.2	108	10.1	1.4	46.6×10^5

TABLE 1. Free-stream conditions at the exit plane of the nozzle

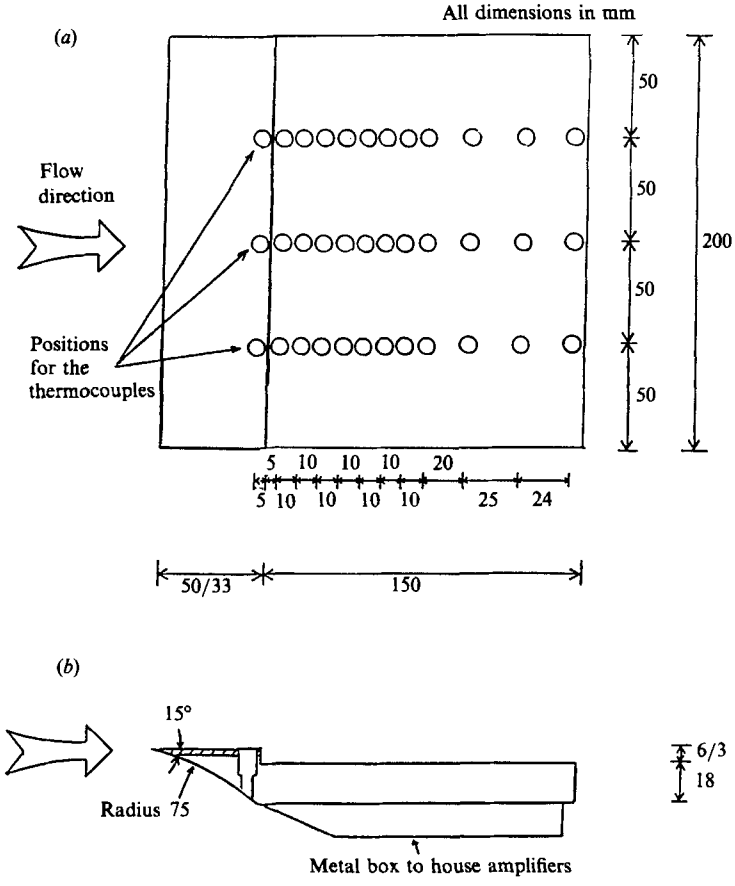

FIGURE 1. The rearward-facing step model.

configurations was 1 and 1.09 respectively. This may be compared with the values of 2.57 (Rom & Seginer 1964), 1.378 (Sandford & Ginoux 1968) and 0.65 (Wada & Inoue 1973) used in the previous investigations.

Surface thermocouples to measure heat-transfer rates were positioned both upstream of the step and in a series of positions downstream of the step. At any one time five thermocouples could be placed at desired locations as shown in figure 1. The thermocouples were then connected to amplifiers located in a metal housing just under the model.

The miniature surface thermocouples used in these experiments were similar to

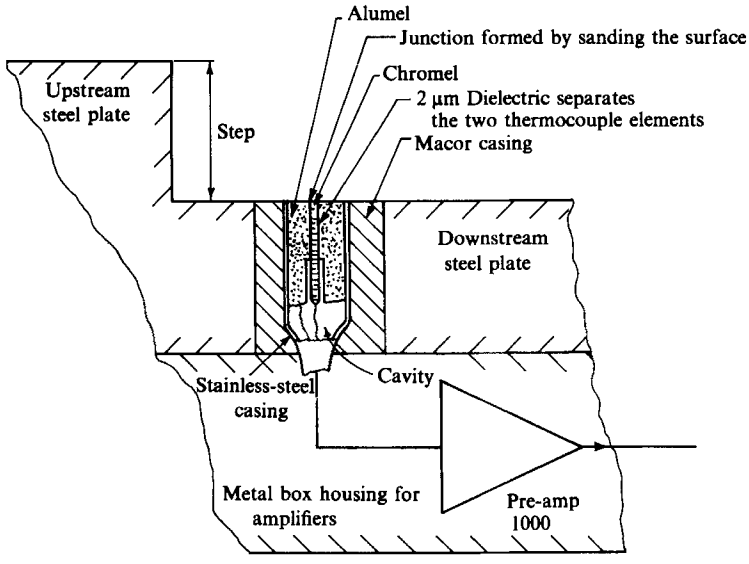

FIGURE 2. Details showing thermocouple/amplifier assembly.

those used by Roberts (1984) in the present facility for measuring heat transfer rates in dusty and non-dusty gases. These thermocouples, of type YL641015 by ASEA Corporation of Sweden, are specially designed to operate in hostile environments of very high temperatures and pressures.

A typical thermocouple assembly as mounted in the model is shown in figure 2. It consists of a type K (Chromel–Alumel) thermocouple of coaxial symmetry sheathed in a stainless-steel casing. A rise time of ~ 1 μs is claimed owing to the very thin (~ 2 μm) dielectric separating the two thermocouple elements, enclosed in Macor sleeves (for electrical isolation), and then the whole assembly is mounted in the model.

2.3. *Mach–Zehnder interferometer*

The flow field over the model was recorded using a Mach–Zehnder interferometer with a field of view of 200 mm diameter. The fringe width was adjusted to be a fraction of the step height so that adequate resolution was obtainable. The light source was a filtered flash lamp with a pulse width of about 1 μs so that stationary fringes could be obtained in a steady flow of about 300 μs. The finite-fringe mode was preferred to an infinite-fringe mode because of the intensity variation across the field of the light source. If an infinite-fringe mode had been used, the intensity variation would have caused a calibration problem when interpreting fringe shifts with a magnitude of less than a fraction of fringe width. However, some infinite-fringe photographs were obtained for comparison purposes.

3. Data processing and accuracy of heat-transfer measurements

Since the thermocouples monitor surface temperatures, they may be regarded as semi-infinite in mass so that it is possible to calculate the heat transfer rate $\dot{q}$ in real time using an R-C analog network which simulates the flow of heat into a substrate. The 'semi-infinite' assumption is valid for these run times (~ 300 μs) since the thermal penetration depth is very small compared with the thermocouple dimensions

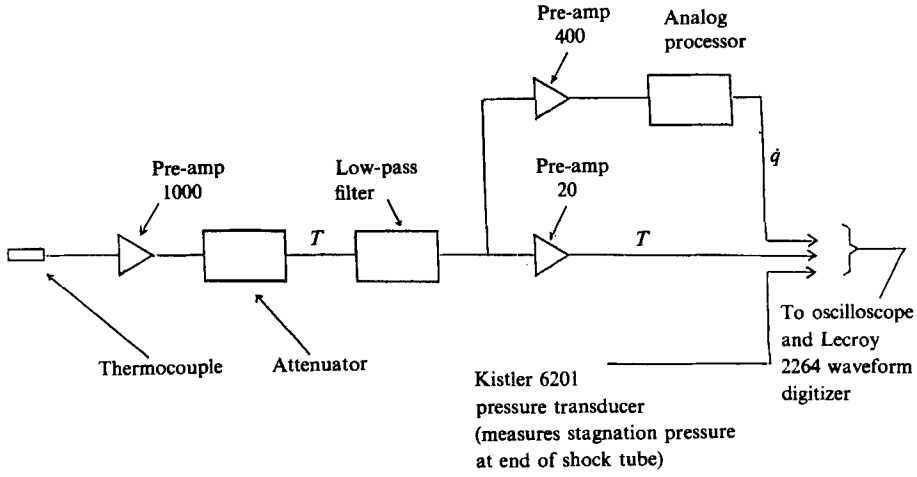

FIGURE 3. Schematic of the data acquisition and processing system.

(Schultz & Jones 1973). The output of the electric analog is then proportional to $\dot{q}$. The design was based on that of Schultz & Jones (1973) with a bandwidth of 10^2–10^5 Hz and a response time of the order of 6 μs.

Since the output of the thermocouple was only 40 μV/K, a low-noise differential amplifier was incorporated into the design and was located inside the model. The signal was then conditioned externally using attenuation where necessary, and a low-pass filter with a roll-off of 12 dB per octave above 15 kHz.

The filtered and unfiltered temperature and heat-transfer signals were recorded using a LeCroy 2264 waveform digitizer. This has a 32 K memory and samples at a rate of 400 kHz when handling 8 multiplexed channels. This yields a total memory of 10.24 ms per channel, which was adjusted so that thermocouple signals began halfway through this period. The instrument contains an A/D converter which was used to display the memory contents on an oscilloscope for recording on a Polaroid film. The schematic of the data acquisition and processing is shown in figure 3. Figure 4 shows a comparison of the output from a typical thin film gauge and the surface thermocouple. It is seen that the surface thermocouple responds as well as the thin film gauge and the signal also is quite clean.

Following Schultz & Jones (1973), the heat-transfer rate $\dot{q}$ is expressed as

$$\dot{q} = (\rho ck)^{\frac{1}{2}} \Delta T_s \frac{1}{R_1} (r'/c_1)^{\frac{1}{2}}, \tag{1}$$

where ΔT_s is the temperature rise obtained from the thermocouple, and ρ, c, k are the density, specific heat capacity and thermal conductivity of the gauge while $(1/R_1)$ $(r'/c_1)^{\frac{1}{2}}$ is the calibration factor of the analog circuit.

The thermal product $(\rho ck)^{\frac{1}{2}}$ was calibrated to be 9997 J/m^{2}Ks$^{\frac{1}{2}}$ which differs by less than 0.5% from the value used by Roberts (1984). The calibration method uses an optical technique, is simple and gives results which compare very well with those obtained using the usual electrical methods, and is suitable for both thin-film-type and thermocouple-type gauges. More details may be found in Lyons & Gai (1988).

The temperature rise ΔT_s is $\Delta V/\beta$, where β, the voltage change per unit rise in temperature, is 40 μV/K. The quantity $(1/R_1)(r'/c_1)^{\frac{1}{2}}$ was calibrated to be 950 s$^{\frac{1}{2}}$.

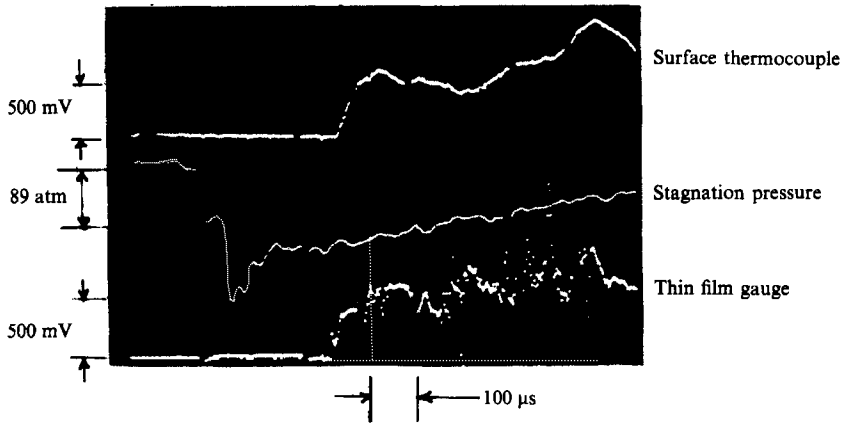

FIGURE 4. Comparison of output from the thin film gauge and the surface thermocouple.

The present measurements have been carried out within the enthalpy range for which an extensive data base has been established over a period of time (R. J. Stalker 1982, personal communication). The calculated and measured accuracies of free-stream stagnation enthalpy and Pitot pressure are of the order of $\pm 10\%$ and $\pm 8\%$ respectively. Based on this, it is estimated that heat-transfer measurements are accurate to $\pm 15\%$.

4. Results and discussion of heat-transfer measurements

4.1. *Upstream flat-plate heat transfer*

Three positions were available on the upstream flat-plate part of the model, just ahead of the step, to measure heat-transfer rates. These were used first to check the validity of two-dimensionality of the flow and secondly to compare the present values with those of East *et al.* (1980) which were obtained under similar flow conditions. Figure 5 shows traces to indicate the two-dimensionality of the flow in the mid-span region of the model.

We note that traces along the centreline, of stagnation pressure, surface temperature rise and heat transfer rate are almost identical to those measured off-axis at a distance of 50 mm towards the side edge of the plate. Since the measurements were taken just upstream of the step, it is reasonable to assume that the oncoming flow is reasonably two-dimensional in the mid-span region. These measurements were repeated at least three to four times and the results were found to be consistent.

Both Rom & Seginer (1964) and Wada & Inoue (1973) have commented on the two-dimensionality of the flow in their experiments. In Rom & Seginer's case, the model spanned the test section and the two-dimensionality was mainly confirmed by the fact that measurements were repeatable within the experimental scatter, which they point out would not normally be the case if there were serious three-dimensional effects.

In the case of Wada & Inoue (1973), the experimental arrangement was similar to the present one in that the model had a finite span with free ends and was exposed to the flow at the exit plane of the nozzle. Measurements made on the centreline of the model and off-axis showed good agreement within the experimental accuracy and they concluded that the flow was two-dimensional.

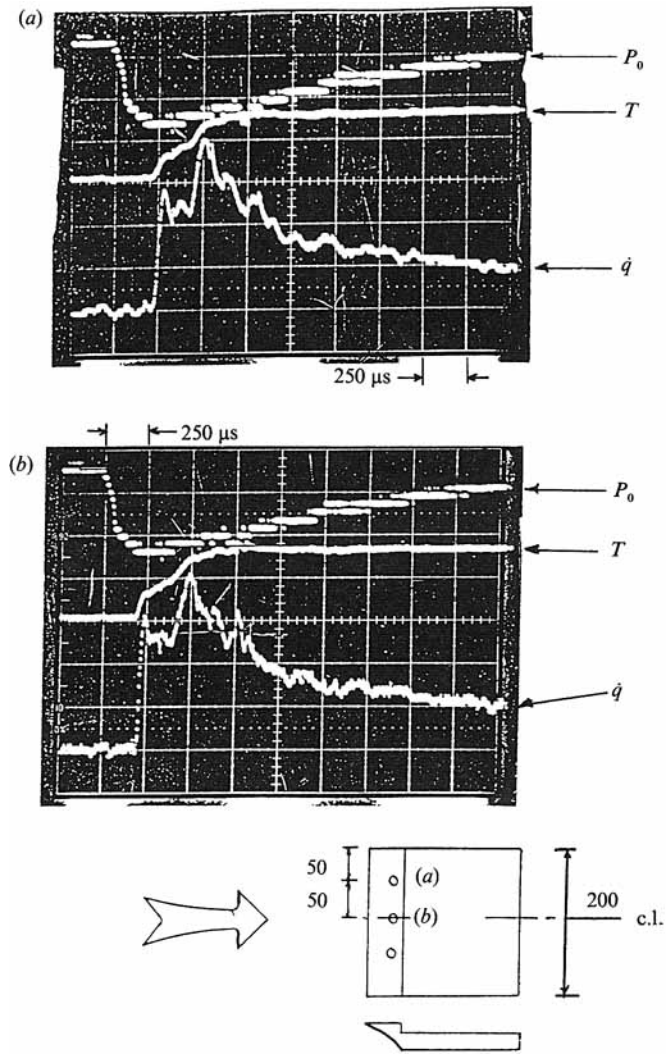

FIGURE 5. Photographic traces showing heat-transfer traces upstream of the step to establish the two-dimensionality of flow.

For the present experimental arrangement the aspect ratio is higher than that of Wada & Inoue (1973). Also, the model was within the inviscid core of the nozzle. These considerations, and the fact that at high Mach numbers the aspect-ratio effects become less important, would suggest that three-dimensional effects are not serious, at least in the central portion of the plate where measurements are taken. Further, in their study of flow over a flat plate with forward-facing step at $M = 2$ and zero incidence in an open-jet low-density wind tunnel, Rogers, Metcalf & Berry (1967) conducted some tests to study the influence of the width of the plate on the centreline pressure distribution to verify the two-dimensionality assumption. Their results showed that the use of a smaller span plate (with an aspect ratio of 0.58) did not give significantly different results. All one can say, therefore, is that so long as the measurements taken in the central portion of the flow field are self-consistent, one can accept the results as at least a fair approximation to two-dimensional flow conditions.

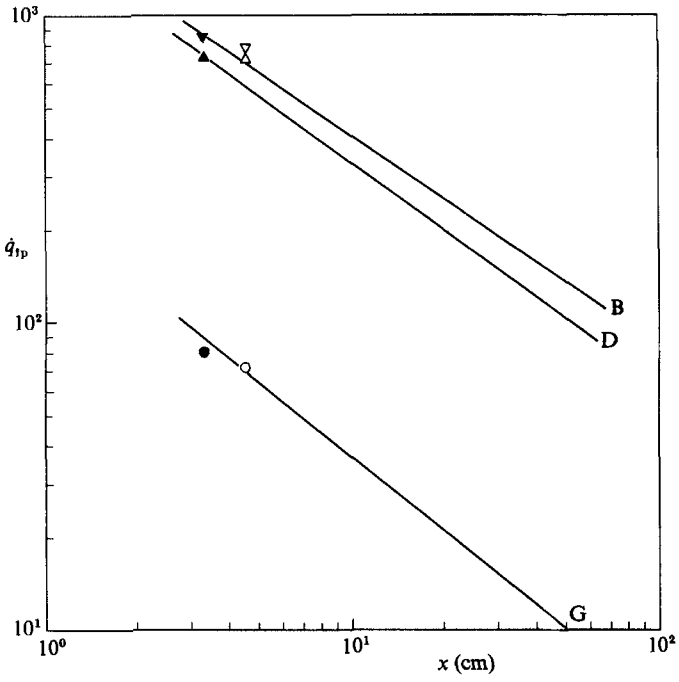

FIGURE 6. Flat-plate heat-transfer data: straight line through experimental data of East *et al.* (1980); ○(G), △(D), ▽(B), data by Reynolds (1985); filled symbols, data by Ross (1986).

Figure 6 shows a comparison between the values obtained by East *et al.* (1980) and the present data for the flat plate. It is seen that the values compare well for all the three run conditions. This also provided an indirect confirmation that the results obtained from the surface thermocouples are in satisfactory agreement with those obtained by thin film gauges.

4.2. *The boundary layer at the step corner*

There is sufficient evidence that both heat transfer and pressure distribution behind the step are very strongly influenced by the boundary layer just before separation, especially its thickness in comparison to the step height (see for example, Charwat *et al.* 1961*a*, Rom & Seginer 1964). It is therefore of interest to have an estimate of the boundary-layer thickness just before separation. Since there was no provision to directly measure the boundary-layer thickness, it had to be deduced indirectly.

Assuming the air to be an undissociated perfect gas, it is possible to calculate the boundary-layer thickness using Eckert's reference-temperature method (White 1977). Estimates made on this basis are indicated in figure 7 for the three enthalpies used in the tests. However, it was possible to estimate the thermal-boundary-layer thickness (δ_T) from the phase map of the flow deduced from the interferograms (for details see under flow visualization in §5) and these are also shown in figure 7. Now Baird, Lyons & Gai (1985) have studied flat-plate non-equilibrium laminar hypersonic boundary layers in air in the same facility at various flow conditions including the present ones. Using Pitot measurements and M-Z interferometry, they obtained velocity and density profiles and could thus obtain the thicknesses of velocity-boundary-layer thickness (δ_V) and the thermal-boundary-layer thickness (δ_T). These results show that, for a dissociated laminar boundary layer on a flat plate,

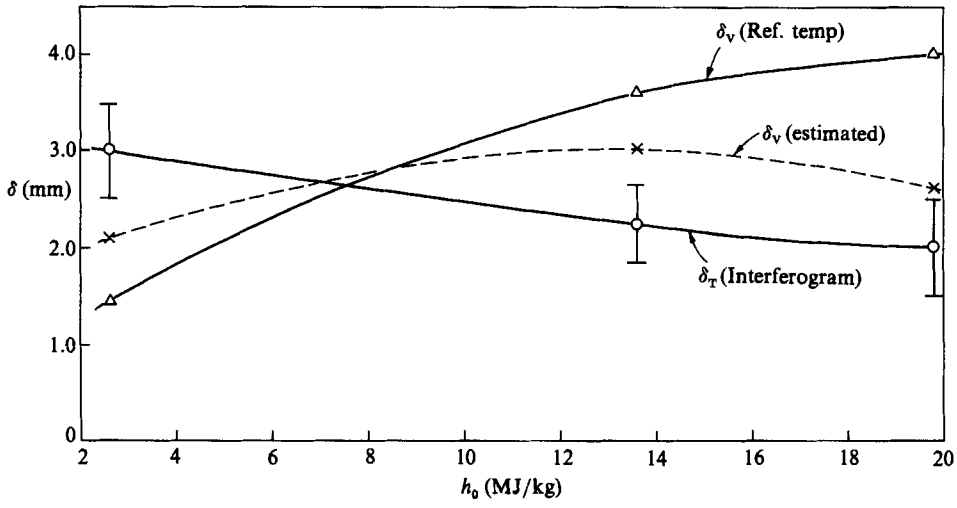

FIGURE 7. Estimation of the boundary-layer thickness at separation. Upstream flat-plate length $L = 50$ mm.

the velocity boundary layer is thicker than the thermal boundary layer (in other words, the Prandtl number is greater than unity), while for an undissociated boundary layer the thermal-boundary-layer thickness is slightly greater than the velocity-boundary-layer thickness (that is, Prandtl number is slightly less than unity). Using this data, therefore, it was possible to estimate the velocity-boundary-layer thickness for the three flow conditions B, D and G. These are also shown in figure 7. It is at once seen that these values fall between those from the reference-temperature method and flow-visualization data.

Figure 8 shows the boundary-layer thickness (δ_s) variation for the two lengths of 50 mm and 33 mm corresponding to step heights (h) of 6 mm and 3 mm respectively. Based on these estimates, δ_s/h ranged between 0.35 and 0.81 for all the tests and thus varied from less than to near unity.

When the boundary-layer thickness is comparable with the step height, $\delta_s/h \sim 1$, results by Rom & Seginer (1964) showed that the heat-transfer distribution behind the step is smooth and the reattachment process is gradual. If the boundary layer at separation is thin compared with step height ($\delta_s/h \ll 1$), then owing to higher local velocity gradients, the heat-transfer distribution is steep and the reattachment heat transfer has a discernible peak. A similar behaviour with pressure distribution was observed by Charwat *et al.* (1961*a*).

4.3. *Heat transfer behind the step*

As has been pointed out, the boundary-layer thickness at separation represents an important lengthscale for separated and near-wake flows. Rom & Seginer (1964) further find that the local heat transfer and flow field are not strongly dependent on wall-temperature ratio. A slight Mach-number effect is evident from previous investigations (Rom & Seginer 1964; Charwat *et al.* 1961*b*) but there is evidence to suggest that this may reflect in the variation of δ_s/h, rather than the free-stream Mach number itself. Also, as discussed in §4.1, the effect of finite aspect ratio should also be small. Thus, if $\dot{q}_{fp}$ is the heat-transfer rate upstream of the step just before

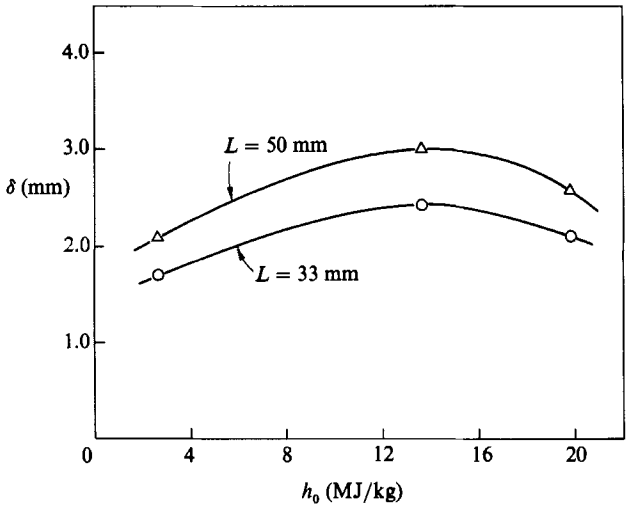

FIGURE 8. Boundary-layer thickness at separation with $L = 50$ mm and $L = 33$ mm.

separation and $\dot{q}$ is the local heat-transfer rate in the separated region behind the step,

$$\frac{\dot{q}}{\dot{q}_{\mathrm{fp}}} = F\left(\frac{\delta_{\mathrm{s}}}{h}\right). \tag{2}$$

For a laminar boundary layer, $\delta_{\mathrm{s}} \sim L/Re_L^{\frac{1}{2}}$, where Re_L is the Reynolds number based on free-stream conditions and the upstream flat-plate length L. Then,

$$\frac{\dot{q}}{\dot{q}_{\mathrm{fp}}} = F\left(\frac{L}{hRe_L^{\frac{1}{2}}}\right). \tag{3}$$

Both Rom & Seginer (1964) and Wada & Inoue (1973) found that not only is the local heat-transfer distribution dependent on the parameter $L/hRe_L^{\frac{1}{2}}$ but also that the type of heat-transfer distribution obtained depended on its value. In particular, if $L/hRe_L^{\frac{1}{2}}$ is greater than a certain value, then the distribution is such as to show gradual increase in heat-transfer rate up to reattachment and attaining a near constant value thereafter; otherwise, the heat-transfer distribution rise is quite abrupt and reaches a peak in the vicinity of reattachment. Also, heat-transfer rates in this case can be many times higher than the laminar flat-plate values.

It would appear from the investigations of Rom & Seginer (1964) and Wada & Inoue (1973) that the value of the parameter $L/hRe_L^{\frac{1}{2}}$ delineating the boundary between the two types of heat-transfer distributions is dependent on whether the flow is supersonic or hypersonic. Thus, from Rom & Seginer's results we find that in supersonic flow the two types of heat-transfer distributions described above occurred depending on whether $L/hRe_L^{\frac{1}{2}} \gtrless 0.067$. In Wada & Inoue's experiments, which were conducted in a hypersonic gun tunnel at a Mach number of about 10, the delineating value of the parameter was about 0.03.

The parameter $L/hRe_L^{\frac{1}{2}}$ takes account of both the free-stream effect and the flow geometry as defined by the ratio L/h. Therefore, in order to study its effect on heat transfer, it is desirable to have as large a range as possible. In the case of Rom & Seginer (1964) this variation of $L/hRe_L^{\frac{1}{2}}$ was achieved by keeping L/h constant and varying free-stream conditions (hence Re_L) by a large variation in shock-tube

pressures. In the case of Wada & Inoue (1973), however, while there was some variation in the free-stream-based unit Reynolds number, variation in $L/hRe_L^{\frac{1}{2}}$ was mainly achieved through a change in the ratio L/h. In the present instance, variation in $L/hRe_L^{\frac{1}{2}}$ is achieved first by varying run conditions at a given L/h and then changing the latter for given run conditions. This gave a change in $L/hRe_L^{\frac{1}{2}}$ from 0.017 to 0.112 which falls within the range covered by the above investigators.

As has been pointed out earlier, the free stream is a frozen dissociated flow for the two high-enthalpy conditions B and D and it is undissociated for condition G. The fluid mechanics of the problem would, therefore, be expected to be governed by the parameter $L/hRe_L^{\frac{1}{2}}$. A further discussion of these aspects is given in §6.

In non-dimensionalizing the local heat-transfer rates in the separated region behind the step, a question arises as to what reference value to use. Some investigators in the past, notably Chapman (1956), Rom & Seginer (1964) and Wada & Inoue (1973), have used the local heat transfer value $\dot{q}_x$ that would exist at the same location with an attached boundary layer in the absence of the step. This simply means extending the length of the flat surface for boundary-layer growth from the leading edge.

On the other hand, some authors both in theoretical and experimental investigations of separated flows (see for example, Charwat *et al.* 1961*b*; Naysmith 1961; Baker & Martin 1966; Wyborny, Kabelitz & Schepers 1967) have used the heat-transfer rate at the step corner just before separation. From the point of view of engineering applications one is interested to know the heat transfer in a separated region compared to its value ahead of separation where the flow is attached, so that the more appropriate reference value to us seems to be that just ahead of separation. In any case, this method of presentation of data would differ from the other only in terms of a (lower) multiplication factor. In the present instance, therefore, we have used the measured heat transfer rate just ahead of the step corner ($\dot{q}_{\mathrm{rfp}}$) as a reference value for non-dimensionalizing the data.

Figure 9 shows results obtained behind steps for the three conditions B, D and G for the two values of L/h ratio and step height tested. Also shown on this figure is the variation of heat transfer for an attached flat-plate boundary layer as deduced from figure 5. We note that the local heat-transfer distribution is dependent on both ($L/hRe_L^{\frac{1}{2}}$) and the step height for a given flow condition.

From this figure we find that the location downstream of the step where the separated-flow heat transfer reaches the attached flat-plate value increases for the larger step height. Secondly, local heat-transfer rates for the larger step height are generally 50% lower.

Figure 10 (*a*, *b*) shows the effect of changing free-stream conditions for a given flow geometry as defined by the L/h ratio and the step height. First, figure 10 (*a*) shows that in the separated region, immediately behind the step, the lower the Reynolds number, the higher the heat-transfer rate; also, the increase downstream of the step is steeper, the lower the Reynolds number.

Figure 10 (*b*) shows similar features but heat-transfer rates are much closer to each other and the plateau-like region is more well defined. Far downstream, heat transfer rises appreciably for the (comparatively) high-Reynolds-number condition G.

Figure 11 (*a*) compares a set of data from the present tests with those by Wada & Inoue (1973) in terms of the $L/hRe_L^{\frac{1}{2}}$ parameter and the heat-transfer rate non-dimensionalized with the corresponding attached flat-plate value $\dot{q}_{\mathrm{rfp}}$. The step height in both cases is the same.

Comparison with the data of Wada & Inoue (1973) is useful because their tests

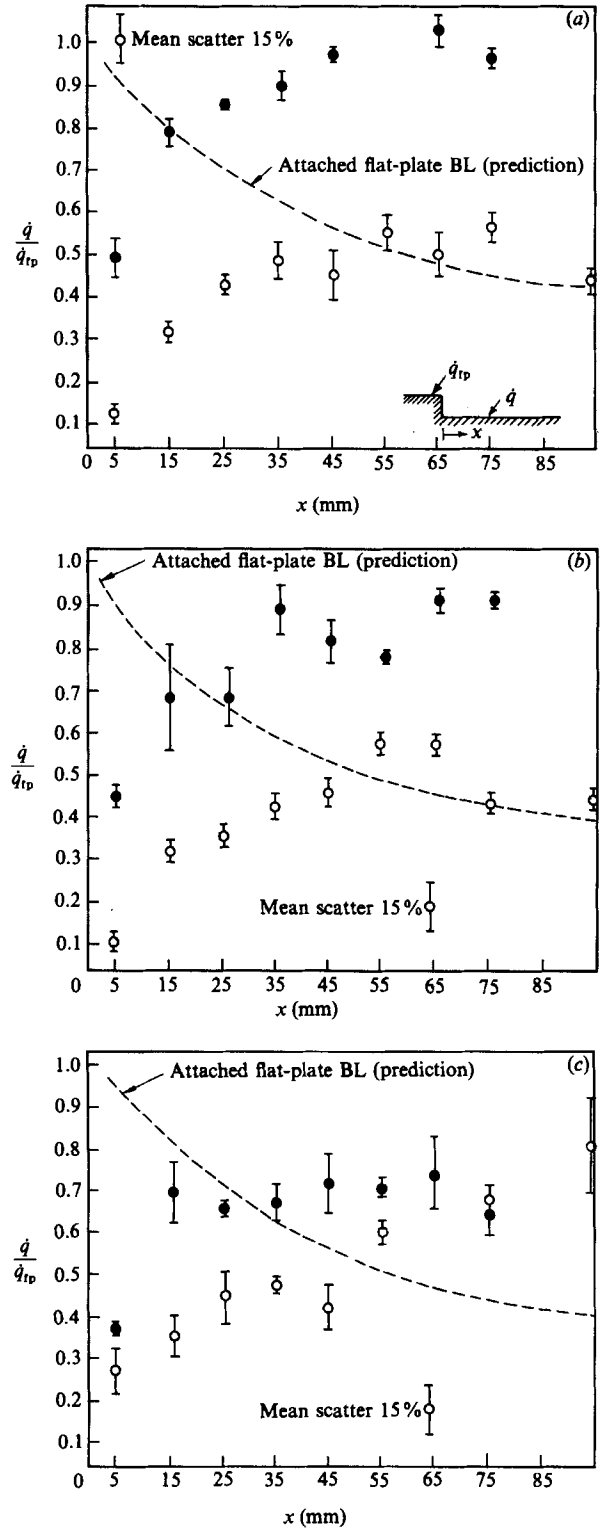

FIGURE 9. Heat-transfer variation downstream of the step. (*a*) Condition B: ●, $h = 3$ mm, $L/h = 11$, $L/hRe_L^{\frac{1}{3}} = 0.112$; ○, $h = 6$ mm, $L/h = 8.33$, $L/hRe_L^{\frac{1}{3}} = 0.069$. (*b*) Condition D: ●, $h = 3$ mm, $L/h = 11$, $L/hRe_L^{\frac{1}{3}} = 0.10$; ○, $h = 6$ mm, $L/h = 8.33$, $L/hRe_L^{\frac{1}{3}} = 0.065$. (*c*) Condition G: ●, $h = 3$ mm, $L/h = 11$, $L/hRe_L^{\frac{1}{3}} = 0.028$; ○, $h = 6$ mm, $L/h = 8.33$, $L/hRe_L^{\frac{1}{3}} = 0.017$.

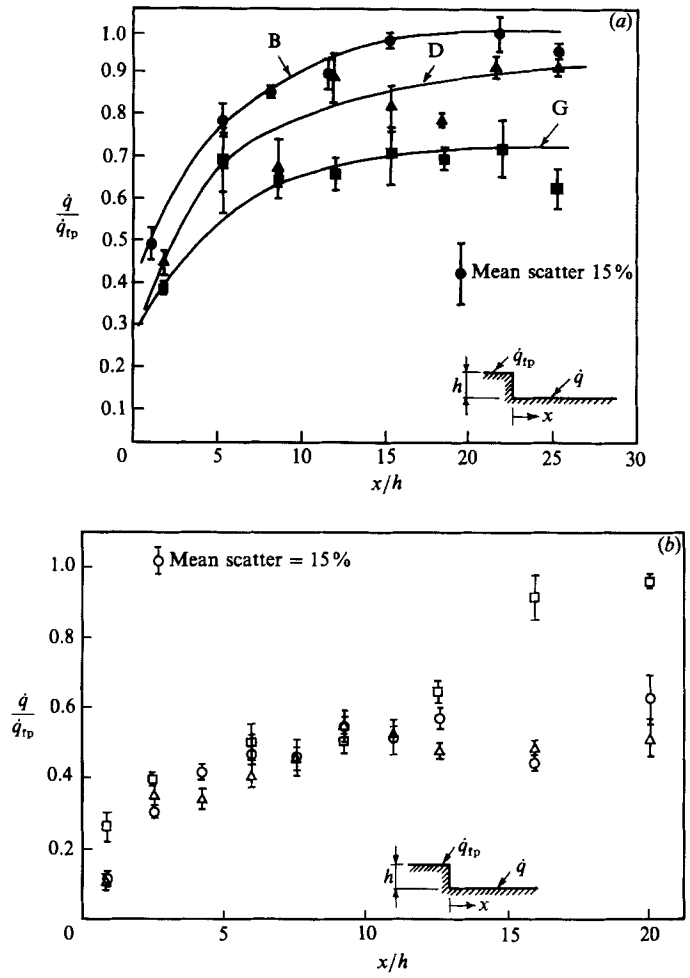

FIGURE 10. Heat transfer downstream of the step. (*a*) $h = 3$ mm; $L/H = 11$: ● (B), $Re_L = 0.97 \times 10^4$; ▲ (D), $Re_L = 1.2 \times 10^4$; ■ (G), $Re_L = 15.7 \times 10^4$. (*b*) $h = 6$ mm; $L/h = 8.33$: ○ (B), $Re_L = 2.1 \times 10^4$; △ (D), $Re_L = 2.3 \times 10^4$; □ (G), $Re_L = 23.2 \times 10^4$.

were conducted similarly at high Mach numbers in a hypersonic gun tunnel in a free stream generated by a conical nozzle and using similar instrumentation techniques. Theirs differ from the present data only in that the enthalpies were much lower and the flow exhibited no dissociation effects.

These results show some interesting features. First consider the case of $L/hRe_L^{\frac{1}{3}} = 0.028$. For both sets of data the ratio L/h is nearly the same and the flow is undissociated. We note that the peak in heat transfer for the present results is higher and occurs further downstream compared to the results of Wada & Inoue (1973). The peak value is nearly 1.5 times the flat-plate value while Wada & Inoue's results show a peak at slightly greater than unity. The only difference in these sets of data is the Reynolds number Re_L as indicated on the figure.

Present results at a higher value of the parameter $L/hRe_L^{\frac{1}{3}}(= 0.112)$ with L/h remaining the same show that heat-transfer rates are now much higher and also there appears to be no distinct peak even as far downstream as 25 step heights. The Reynolds number Re_L, of course, is now much lower so there appears to be some

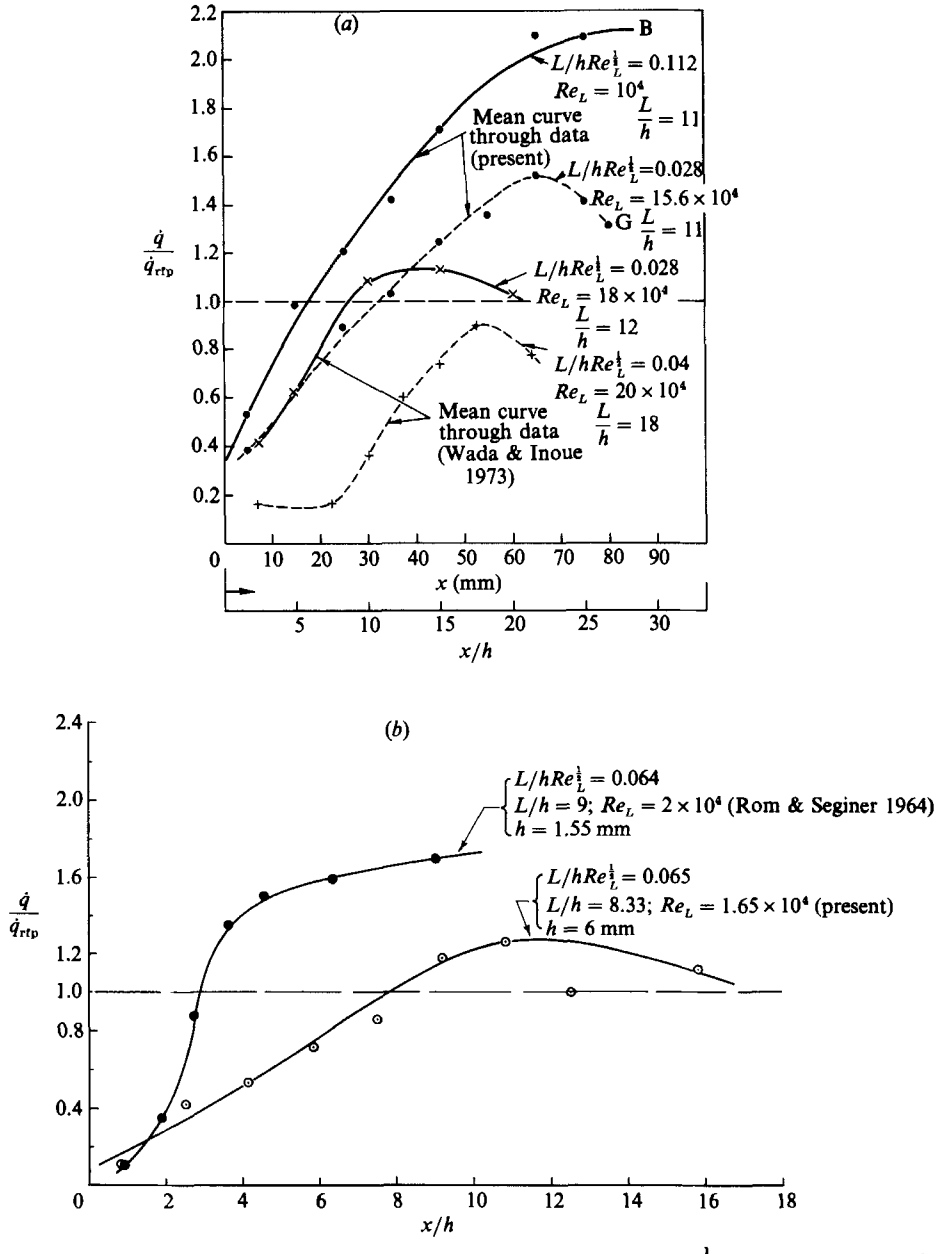

FIGURE 11. (*a*) Comparison of heat-transfer data in terms of $L/hRe_L^{\frac{1}{4}}$. (*b*) Comparison of data showing influence of step height.

Reynolds-number effect. It would appear, therefore, that for a given flow geometry (that is, for a given L/h and step height) the effect of an increase in the value of the parameter $L/hRe_L^{\frac{1}{4}}$, brought about as a consequence of a decrease in Re_L, would be to shift the location of the heat-transfer peak further downstream. If the Reynolds number Re_L is sufficiently low, there may not be a discernible peak at all in the heat transfer distribution.

Considering now the other set of data by Wada & Inoue (1973), $L/hRe_L^{\frac{1}{4}} = 0.04$,

also shown in figure 11(*a*), it is seen that heat-transfer rates are lower and the peak in heat transfer appears to be located downstream of their $L/hRe_L^{\frac{1}{3}} = 0.028$ data. These measurements, which have a considerable scatter, do not indicate clearly that the peak approaches unity, which it should. The reason is not explained. These data, however, show the effect of increasing the value of the parameter $L/hRe_L^{\frac{1}{3}}$ by changing the geometry (that is, L/h) which is not necessarily the same as increasing $L/hRe_L^{\frac{1}{3}}$ through a change in Re_L via free-stream conditions. Although there is a slight difference in the Re_L, the more significant is the L/h difference.

It would seem, therefore, that while the parameter $L/hRe_L^{\frac{1}{3}}$ is important in the study of heat-transfer distribution behind a step of given height, the way in which it is altered, namely, either by changing the geometry or free-stream conditions, is crucial.

A comment also needs to be made regarding the influence of step height. Wada & Inoue (1973) suggest that the heat-transfer distribution depends not only on the parameter $L/hRe_L^{\frac{1}{3}}$ but also the step height. They came to this conclusion on the basis that, with a larger step height, the location where the heat transfer reaches the laminar flat-plate value is located further downstream and the values of heat transfer immediately downstream of the step after separation are lower than those with smaller step height. A similar observation was made in the discussion with reference to figure 9 earlier. A further elucidation of this point can be made by comparing the present data with those of Rom & Seginer (1964).

Figure 11(*b*) shows these results. It may be noted that $L/hRe_L^{\frac{1}{3}}$ values are about the same. The L/h ratio and the Reynolds number Re_L are also not greatly different. The step heights, of course, are significantly different. We see that the present data with higher step height show overall much lower heat-transfer rates and the peak is located further downstream. It is, therefore, possible that, as Wada & Inoue (1973) have also observed, the heat-transfer distribution behind a step is dependent both on $L/hRe_L^{\frac{1}{3}}$ and the step height h.

Of course, when comparing results of Rom & Seginer (1964) and the present data such as in figure 11(*b*), one should bear in mind the large difference in Mach numbers and the type of flow between the two experiments. Rom & Seginer's experiments were conducted at Mach numbers between 1.5 and 2.5 while the present data have been obtained at hypersonic Mach numbers in a frozen dissociated flow. However, the effect of Mach number, as mentioned earlier, should be reflected in the ratio δ_s/h and, assuming the flow in the separated regions remains frozen (more on this in §6), the difference between the data in figure 11(*b*) is believed to be mainly the effect of step height. Wada & Inoue (1973), on the other hand, attribute to Mach-number effect the difference in the value of the parameter $L/hRe_L^{\frac{1}{3}}$ which delineates the two types of heat-transfer distributions. The present data are not sufficient to warrant such an inference.

It should also be mentioned that Wada & Inoue (1973) do not comment on the nozzle source flow effect on their data. Their experiments were conducted using a conical nozzle of 30 cm diameter with an area ratio of 630 which is almost identical to the present set-up. It is surprising, therefore, that they get such good agreement with theory of their flat-plate data when the flat-plate boundary-layer data of East *et al.* (1980) show much stronger variation than the usual $q \propto x^{-\frac{1}{2}}$ variation, which they have attributed to the conical nozzle source flow effect and which the present results confirm.

5. Flow visualization

Figure 12 shows interferograms of the flow obtained for the three flow conditions. They show the presence of a shock wave off the leading edge, the expansion fan at the corner, the boundary layer on the upstream plate, the separation region behind the step and the reattachment shock. The photographs for run types B and D are not as distinct as for the run type G and this is because of very low densities of the flow behind the step. The imperfections evident on the interferogram are the result of window damage caused during a previous experiment.

Improved visualization is further facilitated by digitizing the interferograms and using Fourier analysis to determine fringe positions. A reference interferogram with no fringe shift (i.e. no flow) is taken immediately prior to each experimental run and this is used to identify the fringe positions for no density change. The interferogram recorded during the run has its fringes shifted owing to density variations occurring with the onset of flow. Both these are then subjected to identical processing as shown in the block diagram of figure 13.

Each of the interferograms were digitized into 512 (points) by 200 (lines) of 8-bit data. The lines were parallel to the direction of flow. Each line was transformed using a fast Fourier technique (FFT) into frequency space and then windowed such that frequencies less than 30 and greater than 180 were set to zero in the first half of the real part of the transform. An equivalent symmetrical window was used in the upper half of the real part of the frequency space and the same mask was used on the imaginary part of the frequency. A reverse transform was then performed and the fringe positions were identified by the zero crossings. A particular central fringe was identified arbitrarily as the zeroth fringe and each other fringe in the line was assigned a consecutive number. Since it was known that the absolute fringe shifts in all parts of the interferogram did not exceed one fringe, no ambiguity was introduced by this process.

Once the fringe positions for the reference and test interferograms were known, the shifts were calculated by subtraction. These values were normalized to the average width of ten fringes in the central section of the line, and the fringe shifts were then colour coded for display. This procedure is also described in Baird, Gai & Reynolds (1986).

Figure 14 (plate 1) shows the results for the three flow conditions. It is immediately apparent that we are now able to pick out more details of the flow field than was possible by looking at the normal interferograms. For example, looking at the photographs, we can clearly see the leading-edge shock wave and the boundary layer on the plate. This latter feature can be seen as the concentration of colours next to the plate upstream of the step. The fact that the colours extend into the region downstream of the step with only a gradual change in width indicates that the gas heated in the boundary layer forms a wake which is a significant feature of the flow downstream of the step.

The boundary-layer wake is distorted by the expansion wave which originates at the step corner and reflects off the leading-edge shock wave. This is evident in condition G, for example, some five step heights downstream.

On the far right-hand side of figure 14 (*a–c*), the reattachment wake shock is just evident. In figure 14 (*a*) for example, it can be seen as a narrow area consisting of two shades of green superimposed on a yellow area.

Density variations are also evident in the free-stream region upstream of the leading-edge shock wave. The divergence of the nozzle flow (15° total angle) causes

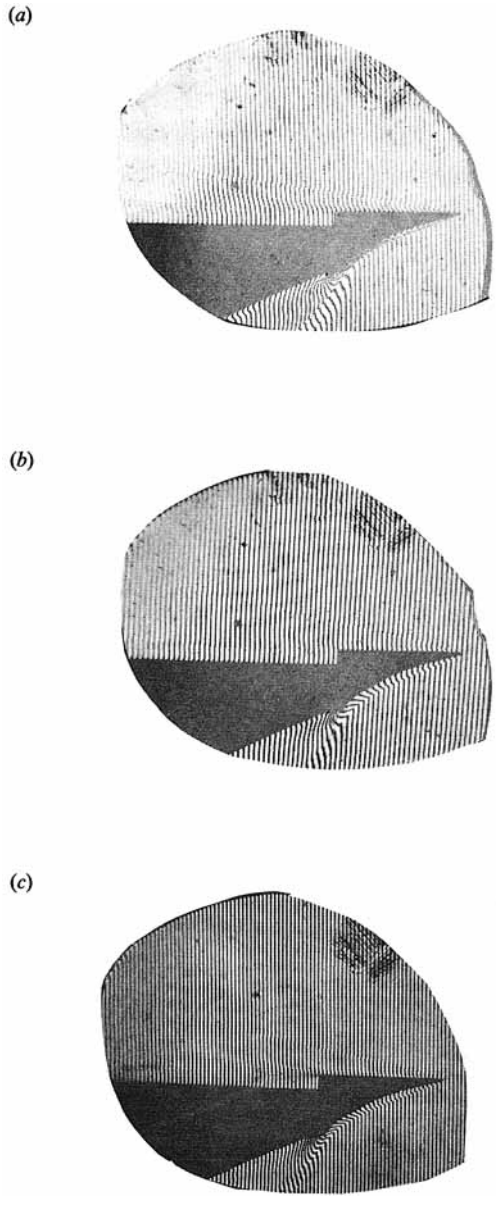

FIGURE 12. Interferograms of the flow: (*a*) condition G; (*b*) condition D; (*c*) condition B.

the integrated density profile to slowly vary in the flow direction. Thus broad colour changes are expected upstream of the shock. Also, as the flow and no-flow interferograms had to be aligned by hand, it was not always possible to obtain exact alignment. The apparent free-stream density variations evident, for example, in figure 14(*b*), are likely to be an alignment problem.

Since the free-stream density is different for each flow condition, a different range of colours is evident in each of the colour plates upstream of the leading-edge shock.

The anamolous horizontal lines in some photographs of figure 14 originated at the window imperfections mentioned previously.

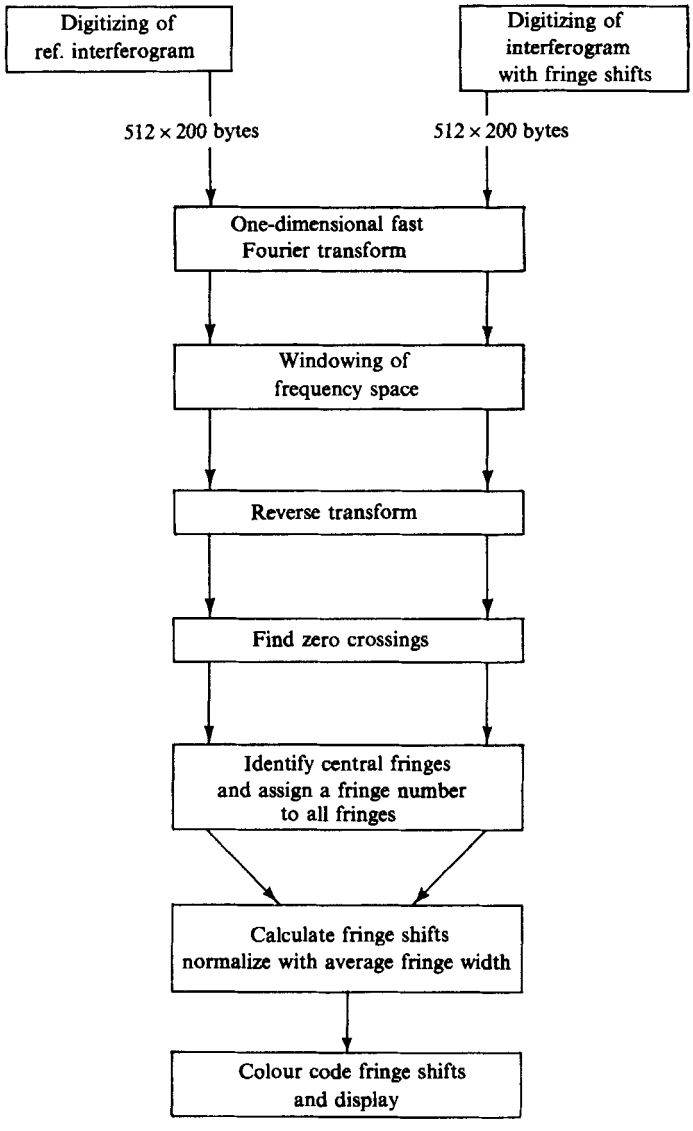

FIGURE 13. Block diagram showing data processing procedure.

6. Further discussion of results

In the present results, while the initial rise and a plateau region indicate a separated region, a strong rise in heat transfer due to reattachment is not evident, except possibly for condition G with 6 mm step height.

There are several reasons for the low heat-transfer rates behind the step. First, so far as the flow upstream of the step is concerned, East *et al.* (1980) have noted that under conditions similar to the present experiments, both gas-phase reactions in the boundary layer and surface reactions on the plate are essentially frozen and the model surface behaved non-catalytically.

When the gas in the boundary layer is frozen, the reaction rate is very slow although its composition may vary by a diffusion process. The heat transfer can still

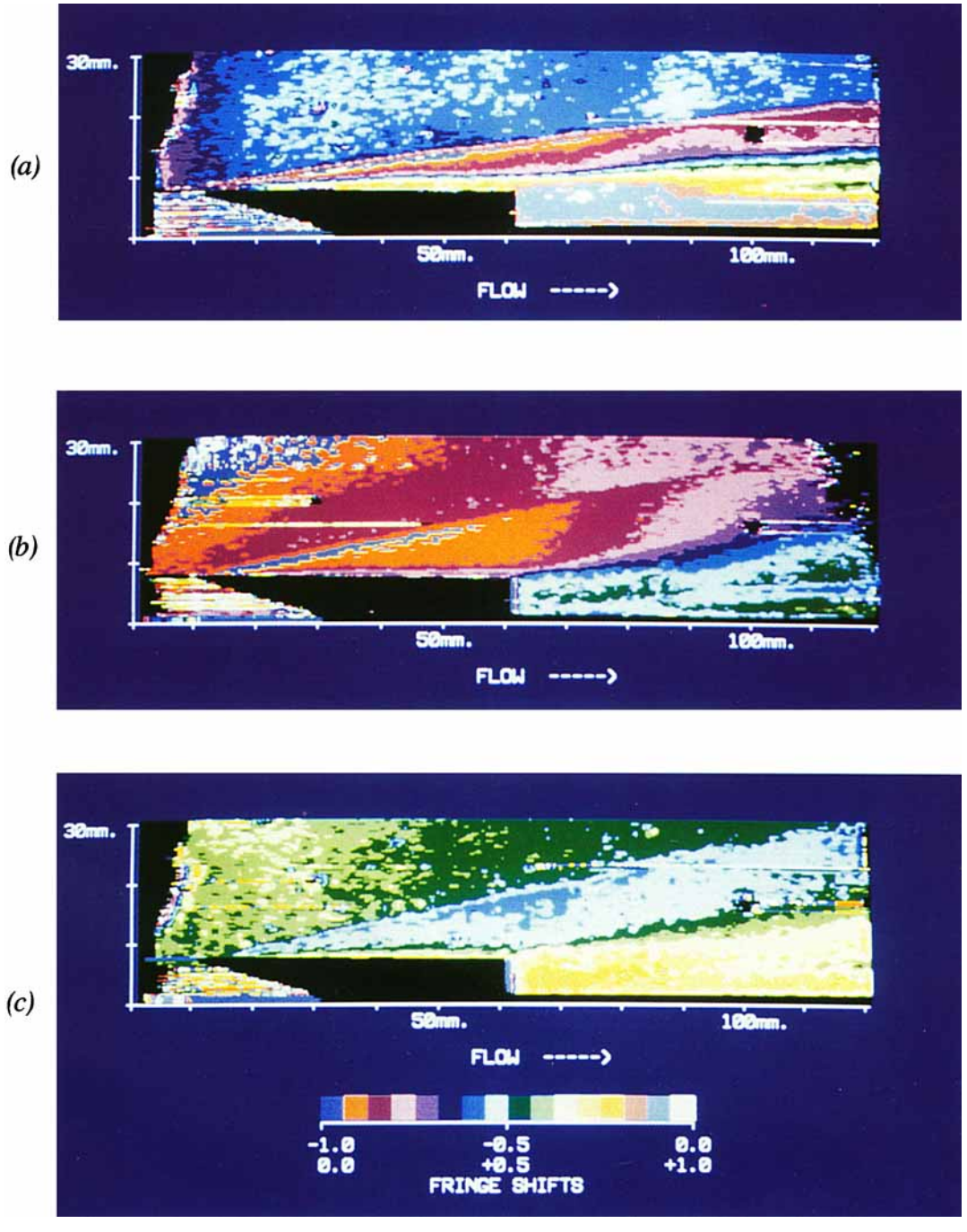

FIGURE 14. Phase map of the flow: colour-coded fringe shifts. *(a)* Condition G; *(b)* condition D; *(c)* condition B.

(*Facing p.* 558)

be affected by catalycity of the model surface. For a fully catalytic wall, all atoms that diffuse to the surface recombine there, depositing their chemical energy on the surface and enhancing the surface heat transfer. If the surface is not fully catalytic, the heat transfer is reduced because of the reduced rate of surface recombination. Thus, the condition of a completely frozen boundary layer and a completely non-catalytic surface represents the lower limit of surface heat transfer.

Secondly, in the present experiments it was shown that upstream flat-plate values of heat transfer were in reasonable agreement with those of East *et al.* (1980). One could therefore infer that similar frozen and non-catalytic behaviour is occurring in the present instance too. Now, downstream of the step the density is further lowered owing to expansion, and since the recombination rate is $\sim \rho^2$ and the boundary-layer surface is the same as the upstream flat plate, the measured heat-transfer rates would represent the frozen boundary layer and non-catalytic surface behaviour.

A possibility, however, exists that the heat-transfer rates immediately behind the step might be affected by the low velocities particularly in the 'dead air' region, which would result in longer residence times of gas particles leading to recombination occurring either in the gas phase or on the surface.†

While a phenomenon like this cannot be ruled out, the short test times of a few hundred microseconds would seem to preclude such a possibility. For example, taking the values of surface and gas-phase Damkohler numbers for conditions B and D as given in East *et al.* (1980), the characteristic surface reaction times (t_w) and characteristic gas-phase reaction times (t_r) work out to be 0.1 s and 1.8–4.3 s respectively so that the boundary-layer gas-phase reactions and surface reactions remain effectively frozen for both atomic oxygen and nitrogen. This is not to say that the present results are unaffected by real-gas effects in the separation and reattachment regions. Significant differences observed between the present data and Wada & Inoue, for example, may still to be a large extent be ascribable to real-gas effects in the present experiments. The present data alone are not sufficient to resolve this point, however.

Reductions in heat-transfer rates behind expansions and increases in the presence of compressions have also been predicted by Back & Cuffel (1970) and Coleman & Stollery (1972). These studies show that, in cold-wall hypersonic flow, the heat transfer is proportional to the mass flux change that occurs across the expansion/compression and is weakly dependent upon the corresponding static temperature drop. It is clear, then, that across the step corner where a strong expansion takes place, the density drop is much more severe than the velocity increase so that a reduction in heat transfer results.

A feature of particular interest is the large plateau-like region and very slow rise in heat transfer in the far downstream region especially for conditions B and D. The reason for this is not clear although it is possible that, because the Reynolds numbers Re_L are very low, the shear layer and the reattached boundary layer would be laminar and very thick. Under such low-Reynolds-number high-Mach-number conditions, the lip shock and the recompression shock would merge within the thick shear layer and a strong recompression shock would not emerge (Hama 1968). Weiss & Weinbaum (1966) also point out that under high-Mach-number low-Reynolds-number conditions, the curvature of the dividing streamline is small and the lip shock strength is also small. The interferograms and the colour-coded phase map of the flow in figures 12 and 14 indeed show that the shear layer downstream of the step

† We are grateful to a referee for alerting us to this possibility.

has very little curvature in it and is almost parallel for quite a long way downstream. Schlieren pictures of Wada & Inoue (1973) as well as those of Richards & Stollery (1979) of laminar flow behind a film cooling slot show similar features.

7. Conclusions

The results have shown that the heat-transfer distribution behind a step depends on the relative thickness of the boundary layer at separation and the step height. This is illustrated through its dependence on the parameter $L/h\,Re_L^{\frac{1}{2}}$ and the step height. In this respect the results are in general agreement with previous investigations, in particular of Rom & Seginer (1964) and Wada & Inoue (1973). However, the importance of flow geometry as defined by the ratio L/h and the Reynolds number Re_L in varying the parameter $L/h\,Re_L^{\frac{1}{2}}$ and therefore the type of heat-transfer distribution obtained, have been elucidated. For all the flow conditions considered the heat-transfer rise was found to be smooth and gradual. Only for the lowest enthalpy condition was there a noticeable peak in the heat-transfer distribution.

Consideration has been given to the real-gas effects that could possibly influence the heat transfer. It is concluded that both the boundary layer on the upstream plate and the separated shear layer downstream of the step remained essentially frozen and the surface was non-catalytic. In this respect, the results agree with those of East *et al.* (1980) obtained under similar experimental conditions.

It is shown that improved flow visualization is facilitated by digitizing the conventional interferograms and using Fourier analysis to determine fringe positions. This is a relatively new technique. The resulting phase map, when colour coded, yields finer details of the flow field which would not otherwise be obvious by ordinary interferometry. The technique, when complemented with other measurements such as heat transfer, leads to improved understanding of complicated flow situations.

The present data have been obtained under high-Mach-number low-density conditions in non-equilibrium dissociated laminar air flows. The range of enthalpies considered was very much greater than those reported previously in the literature.

The paper was written while the first author was on leave at the Engineering Department, University of Cambridge, England. He would like to express his sincere thanks to Dr L. C. Squire for his hospitality and to the Department for providing all the facilities and a stimulating environment.

Grateful acknowledgements are due to the Australian Research Grants Scheme for this support. Thanks are also due to Dr P. Lyons and Mr J. Wie for their assistance in conducting the experiments.

REFERENCES

Back, L. H. & Cuffel, R. F. 1970 *AIAA J.* **8**, 1971–1873.

Baird, J. P., Lyons, P. R. A. & Gai, S. L. 1985 *AIAA 20th Thermophysics Conf., Willamsburg, Virginia, USA.*

Baird, J. P., Gai, S. L. & Reynolds, N. T. 1986. *Proc. 4th Intl Symp. on Flow Visualisation, Paris,* pp. 549–553. Hemisphere.

Baker, P. J. & Martin, B. W. 1986 *Intl J. Heat Mass Transfer* **9**, 1081–1088.

Chapman, D. R. 1956 *NACA Tech. Note* 3792.

Charwat, A. F., Dewey, C. F., Roos, J. N. & Hitz, J. A. 1961*a* *J. Aerospace Sci.* **6**, 457–470.

Charwat, A. F., Dewey, C. F., Roos, J. N. & Hitz, J. A. 1961*b* *J. Aerospace Sci.* **7**, 513–527.

COLEMAN, G. T. & STOLLERY, J. L. 1972 *J. Fluid Mech.* **56**, 741–752.

CRANE, K. C. A. & STALKER, R. J. 1977 *J. Phys.* D *Appl. Phys.* **10**, 679–695.

EAST, R. A., STALKER, R. J. & BAIRD, J. P. 1980 *J. Fluid Mech.* **97**, 673–699.

HAMA, F. R., 1968. *AIAA J.* **6**, 212–219.

LORDI, J. A., MATES, R. E. & MOSELLE, J. R. 1966 *NASA CR*-472.

LYONS, P. R. A. & GAI, S. L. 1988 *J. Phys.* E *Sci. Instrum.* **21**, 445–448.

NAYSMITH, A. 1961 *Proc. Intl Heat Transfer Conf. London*, vol. 43, p. 378. ASME-Inst. Mech. Engrs.

NESTLER, D. E. 1985 *AIAA 20th Thermophysics Conf., Williamsburg, Virginia, USA.*

REYNOLDS, N. T. 1985 Flow over a rearward facing step in high enthalpy hypersonic flow. Final year B.E. thesis.

RICHARDS, B. E. & STOLLERY, J. L. 1979 *J. Aircraft* **16**, 177–181.

ROBERTS, G. T. 1984 *University of Southampton, Rep. AASU Mem.* 84/7.

ROGERS, E. W. E., METCALF, S. C. & BERRY, C. J. 1967 *Aero. Res. Counc. R&M* 3506.

ROM, J. & SEGINER, A. 1964 *AIAA J.* **2**, 251–255.

ROSS, C. 1986. High Mach number airflow behind a rearward facing step. Final year B.E. thesis.

SANDFORD, J. & GINOUX, J. J. 1968. *Von Karman Institute Tech. Note* 38.

SCHULTZ, D. L. & JONES, T. V. 1973 *AGARD Rep.* 165.

SHANG, J. S. & KORKEGI, R. H. 1968 *AIAA J.* **6**, 986–987.

STALKER, R. J. 1985 *Free piston Shock Tunnel T3, Facility Hand Book*, Univ. of Qld.

WADA, I. & INOUE, Y. 1973 *10th Intl Symp. on Space Tech. and Science, Tokyo.*

WEISS, R. F. & WEINBAUM, S. 1966 *AIAA J.* **4**, 1321–1330.

WHITE, F. M. 1974 *Viscous Fluid Flow*, p. 589. McGraw-Hill.

WYBORNY, W., KABELITZ, H. P. & SCHEPERS, H. J. 1967 *AGARD Conf. Proc.* 19.